

# Multiple cooling episodes in the Central Tarim (Northwest China) revealed by apatite fission track analysis and vitrinite reflectance data

Jian Chang<sup>1,2</sup>  · Nansheng Qiu<sup>1,2</sup> · Xinying Song<sup>1,2</sup> · Huili Li<sup>3</sup>

Received: 21 January 2015 / Accepted: 24 August 2015 / Published online: 3 September 2015  
© Springer-Verlag Berlin Heidelberg 2015

**Abstract** Apatite fission track and vitrinite reflectance are integrated for the first time to study the cooling history in the Central Tarim, northwest China. The paleo-temperature profiles from vitrinite reflectance data of the Z1 and Z11 wells showed a linear relationship with depth, suggesting an approximately 24.8 °C/km paleo-geothermal gradient and 2700–3900 m of erosion during the Early Mesozoic. The measured apatite fission track ages from well Z2 in the Central Tarim range from 39 to 159 Ma and effectively record the Meso–Cenozoic cooling events that occurred in Central Tarim. Moreover, two cooling events at 190–140 Ma in the Early Jurassic–Early Cretaceous and 80–45 Ma in the Late Cretaceous–Paleocene revealed by measured AFT data and thermal modeling results are related to the collisions of the Qiangtang–Lhasa terranes and the Greater India Plate with the southern margin of the Eurasian Plate, respectively. This study provides new insights into the tectonic evolution of the Tarim Basin (and more broadly Central Asia) and for hydrocarbon generation and exploration in the Central Tarim.

**Keywords** Central Tarim · Apatite fission track · Vitrinite reflectance · Cooling events · Tarim Basin

## Introduction

The Tarim Basin is located in the Uygur Autonomous Region of Xinjiang, northwest China (Fig. 1a). It is the largest basin in Central Asia, with an area of  $56 \times 10^4$  km<sup>2</sup>. The Central Tarim, a secondary tectonic unit of the Tarim Basin, is an important oil- and gas-rich area. Some oil–gas fields have already been found here, such as the Tazhong 4 oil field and the Ordovician carbonate condensate gas reservoirs in the No. 1 Fault zone (Fig. 1c). Previous studies indicated that the Tarim Basin experienced multiple uplift and burial episodes since the Late Neo-Proterozoic (Jia 1997; He et al. 2005), which caused difficulty in the understanding of hydrocarbon generation timing in the Central Tarim. Temperature plays an important role in hydrocarbon generation and accumulation; therefore, it is important to reconstruct the tectono-thermal evolution of a region. For the Central Tarim, Xie and Zhou (2002) calculated maximum paleo-temperatures of 119–168 °C for the Cambrian–Ordovician strata using pyrolysis kinetics simulation experiments on samples from the TC1 well (Fig. 1c). Zhang et al. (2011a) obtained Silurian paleo-temperatures for the Central Tarim based on the homogenization temperatures of fluid inclusions. On the basis of vitrinite reflectance ( $R_o$ ) data, Pan et al. (1996) studied the Central Tarim paleo-geothermal gradient evolution, which gradually decreased from 32 to 29 °C/km in the Paleozoic to 26–20 °C/km in the Cenozoic. This research result was very similar to that of Li et al. (2005), who used apatite fission track (AFT) analysis. Qiu et al. (1997) and Xiang et al. (2013) also reported AFT data to discuss tectonic uplift events in the Central Tarim.

Bray et al. (1992) and Green et al. (2002) considered that  $R_o$  values provide discrete estimates of the maximum

✉ Jian Chang  
changjian@cup.edu.cn

<sup>1</sup> State Key Laboratory of Petroleum Resources and Prospecting, China University of Petroleum, Beijing 102249, China

<sup>2</sup> Basin and Reservoir Research Center, China University of Petroleum, Beijing 102249, China

<sup>3</sup> Petroleum Exploration and Production Research Institute, SINOPEC, Beijing 100083, China

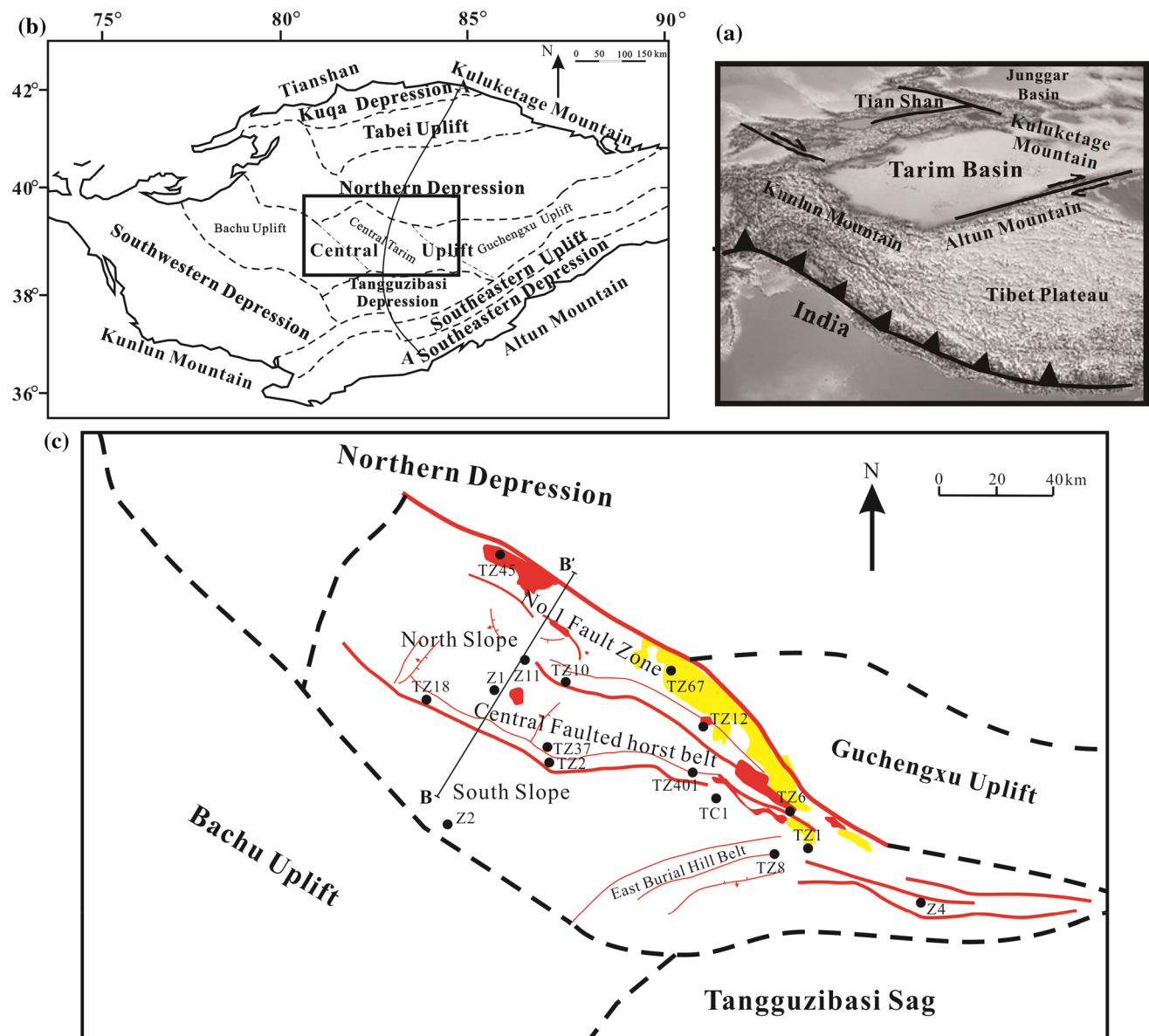


**Fig. 1** **a** Schematic map of central Asia showing the location of the Tarim Basin; **b** sketch map of tectonic units in the Tarim Basin, and the *rectangle box* in its middle means the studied area shown in (c);

**c** the tectonic units, faults and well locations of the Central Tarim (Modified from Li et al. 2010), and the oil and gas reservoir mapping in the Central Tarim referred to Cai (2007)

post-depositional paleo-temperature, whereas AFT may provide lower or upper limits or a range of values for the maximum paleo-temperature in one, two, or rarely three separate episodes. The combination of AFT and  $R_0$  data could provide an independent check on the magnitude of the maximum paleo-temperatures and increase confidence in the paleo-geothermal gradient estimation (Green et al. 2002). A new Paleozoic thermal history of the Tarim Basin was recently reconstructed by integrating AFT and  $R_0$  (Qiu et al. 2012). However, only AFT dating was used to study the Meso–Cenozoic history of the northern margin of the Tarim Basin (Sobel et al. 2006; Wang et al. 2009; Zhang

et al. 2009), and there is little research on the Meso–Cenozoic history of the interior of the Tarim Basin based on the integration of AFT and  $R_0$ . Although AFT and  $R_0$  have been separately applied to the tectono-thermal evolution history of the Central Tarim (Pan et al. 1996; Qiu et al. 1997; Li et al. 2005; Xiang et al. 2013), until now no study has integrated these two methods to study the cooling events and erosion amounts in the Central Tarim. This paper integrates AFT and  $R_0$  data to investigate paleo-geothermal gradients, cooling episodes, and exhumation magnitudes in the Central Tarim. Mesozoic paleo-geothermal gradients of approximately 24.8 °C/km were obtained

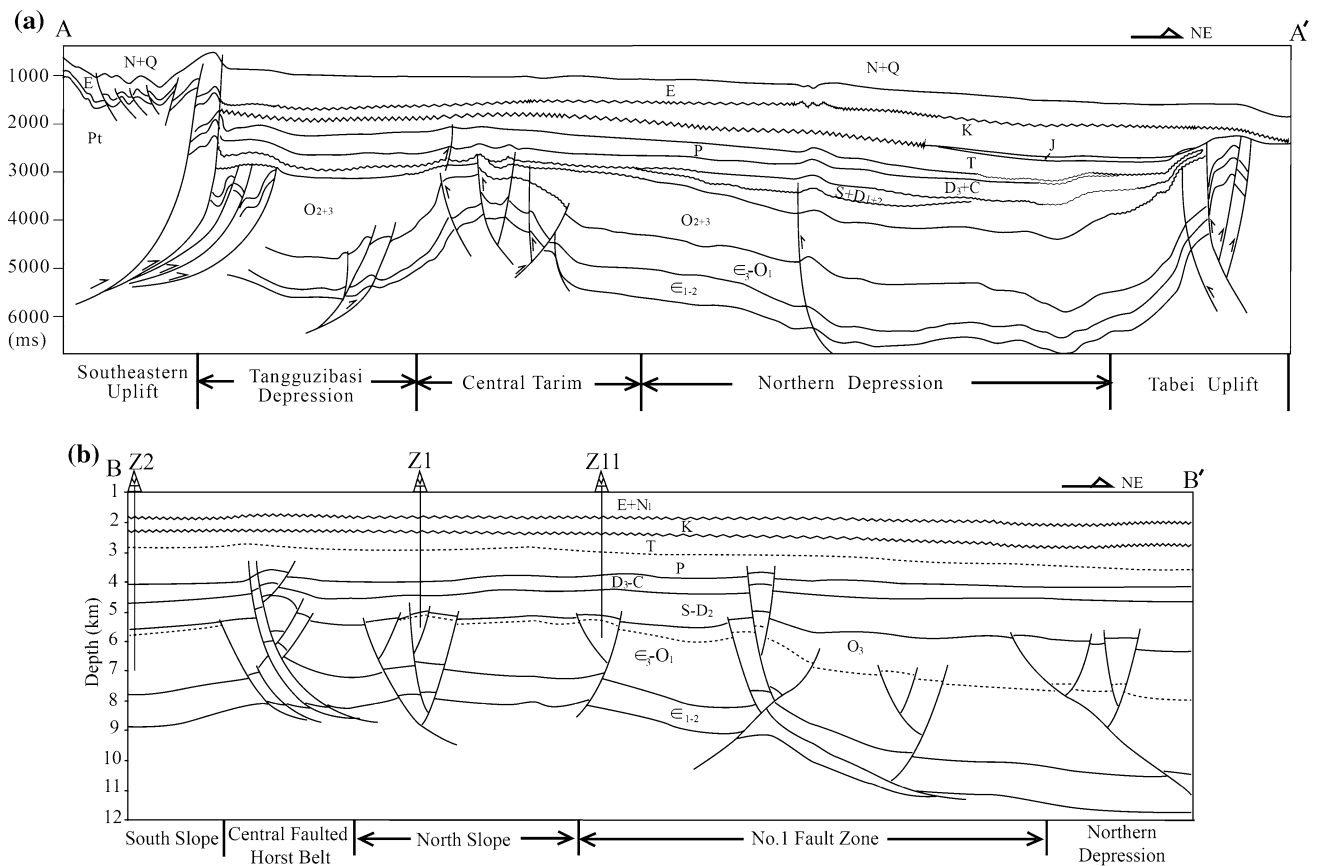


**Fig. 2** Typical cross sections of the Tarim Basin (a) and the Central Tarim (b), which locations were plotted in Fig. 1

from  $R_0$  data from the Z1 and Z11 wells, and two cooling events at 190–140 Ma and 80–45 Ma were revealed by AFT data from well Z2. This study provides a robust and comprehensive analysis of the tectono-thermal evolution of the Central Tarim, which is significant for future hydrocarbon maturation evolution research and oil and gas exploration.

### Geologic setting

The Tarim Basin, one of the most petroliferous basins in China, is bounded by Tian Shan to the north, Kuluketage Mountain to the northeast, Kunlun Mountain to the southwest, and Altun Mountain to the southeast (Fig. 1a). The Tarim Basin is divided into eight structural belts according to basement relief and geophysical features: Kuqa Depression, Tabei Uplift, Northern Depression, Central Uplift, Southeast Uplift, Southeast Depression, Tangguzibasi Depression, and Southwest Depression (Fig. 1b; Jia 1997). The Central Uplift contains three secondary tectonic units: Bachu Uplift, Central Tarim (sometimes known as the Tazhong Uplift), and

Guchengxu Uplift. The crystalline basement of the Tarim Basin formed in the Late Proterozoic (Zhang 2000; He et al. 2005; Wu et al. 2012; Zhang et al. 2013a; Ge et al. 2014). The basement was covered by Early Paleozoic marine carbonate sediments, Late Paleozoic alternating marine and continental sediments, and Meso-Cenozoic terrestrial sediments. The tectonic evolution of the basin was divided into six stages (Jia et al. 1995): (1) cratonic peripheral aulacogen from Late Proterozoic to Ordovician; (2) intracratonic depression from Silurian to Early Carboniferous; (3) intracratonic rift from Middle Carboniferous to Permian; (4) foreland basin stage in the Triassic; (5) intracontinental depression from Jurassic to Paleogene; and (6) recombined foreland basin since the Neogene. As a result of the complex tectonic evolution, five important regional unconformities can be found in the seismic profile (Figs. 2a, 3): (1) Silurian and Ordovician or older strata during the Late Caledonian movement stage II, (2) Carboniferous and Devonian or older strata during the Hercynian movement stage I, (3) Upper Permian–Triassic and underlying strata during the Hercynian movement stage II, (4) Jurassic and Triassic or older strata during the Indosinian movement, and (5) Tertiary

Strata				Thickness (m)	Age (Ma)	Lithology	Tectonic Movement
Era	System	Series	Formation				
Cenozoic	Quaternary(Q)			1195-1460	2.5	Sandstone, Mudstone	Himalayan
	Neogene(N)						
	Paleogene(E)			217-344	23	Sandstone	
Mesozoic	Cretaceous(K)	Lower		189-478	137	Erosion	Yanshan-Indosinian
			Mudstone, sandstone				
	Jurassic(J)			0-541	205	Erosion	
Paleozoic	Triassic(T)			0-541	250	Mudstone, sandstone	
	Permian(P)			0-780	290	Tuff, basalt	Hercynian (II phase)
	Carboniferous (C)	Upper		0-691	350	Erosion	Hercynian (I phase)
		Middle				Marlite	
		Lower				Mudstone interbedded fine sandstone	
	Devonian(D)			0-241	410	Erosion	Late Caledonian (II phase)
	Silurian(S)	Upper		0-517	438	Erosion	Upper mudstone Lower bituminous siltstone
		Middle					
		Lower					
	Ordovician(O)	Upper	Sangtamu	0-748	Erosion	Argillite interbedded sandstone and mudstone	Late Caledonian (I phase)
Lianglitage			0-1000	Erosion	Argilliferous limestone calcarenite, bioclastic grainstone		
Tumuxiuke							
Middle		Yijianfang		Erosion		Middle Caledonian	
Lower		Yingshan	0-2269	490	Erosion	Upper micrite, Lower dolomitic mudstone	early Caledonian
	Penglaiba	Dolomite					
Cambrian(C)	Upper	Qiulitage	1783		Finely crystalline dolomite		
	Middle	Awatage	125		Gypsum interbedded dolomite		
	Lower	Xiaoerbulake	74	543		Finely crystalline dolomite	

**Fig. 3** General stratigraphic column of the Central Tarim (Modified from Li et al. 2010)

and Cretaceous or older strata during the Yanshan and Himalayan movements.

The Central Tarim is an inherited paleo-uplift, which formed during the Late Caledonian–Early Hercynian and has an area of approximately 30,000 km<sup>2</sup> (Fig. 1c; He et al. 2006; Li et al. 2010), which is bounded by the Bachu Uplift to the west, the Guchengxu Uplift to the east, the Northern Depression to the northeast and north, and the Tangguzibasi Depression to the south. The Central Tarim is divided into five structural units according to the distribution of fault systems: No. 1 Fault Zone, North Slope, Central Faulted Horst Belt, South Slope, and East Burial Hill (Fig. 1c). During the Phanerozoic, the Central Tarim evolved from an Early Paleozoic marine carbonate platform to Late Paleozoic alternating marine and continental deposits, and then Meso–Cenozoic continental fluvial sedimentary environments, with average thicknesses of 3500–5000, 1500–2000, and 1500–2500 m, respectively (He et al. 2005; Xiang et al. 2013). According to three-dimensional, high-resolution seismic reflection data, Li et al. (2013) recognized four Paleozoic fault systems in the Central Tarim: (1) Cambrian–Early Ordovician extensional faulting; (2) Late Ordovician NWW trending thrust faulting; (3) Silurian–Devonian NNE strike-slip faulting, and (4) faulting associated with Permian plume. Several obvious unconformities developed in the Central Tarim because of multiple tectonic movements in the Tarim Basin (Fig. 2b). The general stratigraphic column of the Central Tarim is shown in Fig. 3.

The Central Tarim developed in a graben-rift basin with some normal faults from the Late Proterozoic to the Ordovician. Its strata are dominated by carbonate, mudstone, and siltstone rocks (Fig. 3; Lü and Hu 1997; Li et al. 2009, 2013). As a result of the collision between the Kunlun Mountain terrane and the Tarim plate in the Late Ordovician, the Central Tarim experienced tectonic inversion from extension to transpression and began folding and uplifting (Lü and Hu 1997; Wang et al. 1998; Lin et al. 2012). Lin et al. (2012) suggested the Central Tarim and adjacent areas formed an arc-shaped thrust uplift denudation belt during the Late Ordovician. During the Silurian and Devonian, the Central Tarim experienced serious erosion and formed several unconformities as a result of the southward subduction of the South Tian Shan Ocean (Fig. 2b; Wang et al. 1998; Lin et al. 2012). The Central Tarim evolved into a large-scale, westward-plunging-nose uplift during the Carboniferous and Permian (Li et al. 2010), which probably resulted from the closure of the South Tian Shan Ocean in the northern margin of the Tarim Basin. In addition, dramatic magmatic activity during the Early Permian formed a large igneous province in the northwestern Tarim Basin (Yang et al. 2005; Li et al. 2011, 2012); basalt and tuff with U–Pb ages of 290–274 Ma have been found in the Permian formations of many drilling cores in the Central Tarim (Li

et al. 2011, 2012; Zhang et al. 2013b). The Central Tarim experienced further serious erosion during the Meso–Cenozoic; the missing Jurassic and Upper Cretaceous strata are considered as evidence of this (Figs. 2, 3; Wang et al. 1998; Li et al. 2008).

### Vitrinite reflectance ( $R_o$ ) method and data

Vitrinite is a primary component of coals and other organic matter found in sedimentary rocks and often used for reflectance measurements owing to its relatively progressive change in optical properties with increasing temperature (Tissot and Welte 1978). The normal increase in vitrinite reflectance observed in borehole profiles is caused by temperature rising with depth (Stach et al. 1982). Thus, vitrinite reflectance is a reliable parameter for thermal history simulation and can be used to calibrate the amount of erosion in a sedimentary basin. Because vitrinite does not exist in pre-Silurian rocks (Bertrand and Herous 1987), the reflectance of vitrinite-like macerals and bitumen in Cambrian–Ordovician sediments is used to evaluate thermal maturation (Bucharadt and Lewan 1990). In this article, all values for vitrinite-like maceral reflectance ( $R_v$ ) and bitumen reflectance ( $R_b$ ) were converted into equivalent vitrinite reflectance values ( $R_{equ}$ ) using the formulae proposed by Wang et al. (1996) and Jacob (1989). The  $R_o$  or  $R_{equ}$  values collected from wells Z1, Z2, and Z11 in the Central Tarim are listed in Table 1. The corresponding paleo-temperature for each  $R_o$  or  $R_{equ}$  value was calculated based on the Easy % $R_o$  model (Table 1; Sweeney and Burnham 1990).

Generally, if heating and cooling are caused by a combination of sedimentation and uplift, the reduced amount of uplift and erosion,  $\Delta Z$ , required to explain the cooling is given by:

$$\Delta Z = (T_i - T_o)/(dT/dZ), \quad (1)$$

where  $\Delta Z$  is the erosion upon the unconformity in meters,  $T_i$  is the paleo-temperature intercept at the unconformity,  $T_o$  is the paleo-surface temperature (20 °C), and  $dT/dZ$  is the paleo-geothermal gradient, which is equal to the slope of a paleo-temperature versus depth linear fitting (Fig. 4a; Bray et al. 1992; Green et al. 2002). The paleo-temperature–depth profile for studied wells should be linear through the preserved section to accurately calculate the geothermal gradient and amount of erosion (Green et al. 2002).

The systematic paleo-temperature data derived from  $R_o$  or  $R_{equ}$  values of Ordovician–Triassic strata in the Z1 and Z11 wells under the unconformity between the Triassic and Cretaceous showed a nice linear relationship with depth. Moreover, the paleo-temperature values were higher than the present-day temperature for the same depth in these wells (Fig. 4), and therefore it is possible

**Table 1**  $R_o$  or equivalent vitrinite reflectance data ( $R_{\text{equ}}$ ) for the wells Z1, Z2 and Z11 in the Central Tarim

Well ID	Depth (m)	Strat.	$R_{\text{equ}}$ (%) <sup>a</sup>	Paleo-temperature (°C)	Well ID	Depth (m)	Strat.	$R_{\text{equ}}$ (%) <sup>a</sup>	Paleo-temperature (°C)
Z1	2670	T	0.71	118	Z2	5439	O	1.55♣	180
Z1	2780	T	0.77	128	Z2	5761	O	1.59♣	182
Z1	2810	T	0.80	131	Z2	5838	O	1.62♣	183
Z1	2890	T	0.82	133	Z2	6150	O	1.68♣	186
Z1	3800	P	0.98	147	Z11	2860	T	0.67	112
Z1	3915	P	1.07	152	Z11	3356	P	0.71	118
Z1	3885	P	0.96	146	Z11	3694	P	0.72	120
Z1	4030	C	1.09	154	Z11	3728	P	0.74	122
Z1	4080	C	1.12	156	Z11	3816	C	0.70	116
Z1	4140	C	1.17	159	Z11	3854	C	0.83	134
Z1	4210	C	1.17	159	Z11	3870	C	0.85	136
Z1	4265	C	1.13	157	Z11	3907	C	0.80	131
Z1	4375	C	1.28	166	Z11	3912	C	0.84	135
Z1	4410	C	1.13	157	Z11	4264	C	0.91	142
Z1	4460	D	1.14	157	Z11	4264	C	0.93	144
Z1	4520	D	1.27	165	Z11	4266	C	0.95	145
Z1	4630	D	1.28	166	Z11	5121	S	1.24♣	164
Z1	4715	D	1.32	168	Z11	5128	O <sub>3</sub>	1.13♣	157
Z1	4785	S	1.32*	168	Z11	5134	O <sub>3</sub>	1.19♣	161
Z1	4815	S	1.35*	170	Z11	5148	O <sub>3</sub>	1.26♣	165
Z1	4885	S	1.36*	170	Z11	5151	O <sub>3</sub>	1.27♣	165
Z1	5010	S	1.36*	170	Z11	5155	O <sub>3</sub>	1.25♣	164
Z1	5090	S	1.37*	171	Z11	5332	O <sub>3</sub>	1.31♣	167
Z1	5205	O	1.50*	178	Z11	5334	O <sub>3</sub>	1.36♣	170
Z1	5215	O	1.63*	184	Z11	5335	O <sub>3</sub>	1.30♣	167
Z1	5350	O	1.60*	183	Z11	5336	O <sub>3</sub>	1.31♣	167
Z1	5430	O	1.70*	187	Z11	5337	O <sub>3</sub>	1.32♣	168
Z1	5520	O	1.69*	187	Z11	5420	O <sub>3</sub>	1.54♣	180
Z1	5560	O	1.75*	189	Z11	5458	O <sub>3</sub>	1.45♣	175
Z2	5287	O	1.43♣	173					

<sup>a</sup> Some vitrinite reflectance ( $R_o$ ) data in the upper Paleozoic and Mesozoic strata are all referred to as  $R_{\text{equ}}$  (equivalent  $R_o$ ) in our study for consistency. The  $R_{\text{equ}}$  values with asterisks (\*) were calculated from vitrinite-like maceral ( $R_v$ ), and  $R_{\text{equ}}$  values with club (♣) were calculated from bitumen reflectance ( $R_b$ ) using the following formulae:  $R_{\text{equ}} = 0.533 R_v + 0.667$  (Wang et al. 1996);  $R_{\text{equ}} = 0.618 R_b + 0.40$  (Jacob 1989). The  $R_o$  or  $R_{\text{equ}}$  data of the well Z1 were modified from Wang et al. (2010), and of which the wells Z2 and Z11 were provided by the Northwest Bureau of Petroleum of SINOPEC

to calculate the paleo-geothermal gradient and amounts of erosion for these wells based on the method of calculating the erosion amount mentioned above. By fitting the linear correlation between the paleo-temperatures and corresponding depths of the Z1 and Z11 wells, we obtained paleo-geothermal gradients (the slopes of the linear fitting correlation) for these two wells of 23.5 and 26.0 °C/km, respectively, after the Triassic (Fig. 4). The corresponding amounts of erosion were calculated based on formula (1) as approximately 3900 and 2750 m for wells Z1 and Z11, respectively. Furthermore, the mean of the paleo-geothermal gradients in wells Z1 and Z11, approximately 24.8 °C/km, is simply regarded as the

Mesozoic geothermal gradient in the Central Tarim based on this work.

### Apatite fission track (AFT) method and data

Apatite fission track thermochronology is based on the accumulation of radiation damage in an apatite crystal owing to the fission decay of  $^{238}\text{U}$  atoms. Fission tracks form continuously through geologic time and anneal over geologic timescales at temperatures above  $110 \pm 10$  °C for most apatite samples (Gleadow et al. 1983; Green et al. 1989). AFT analysis is particularly important to basin

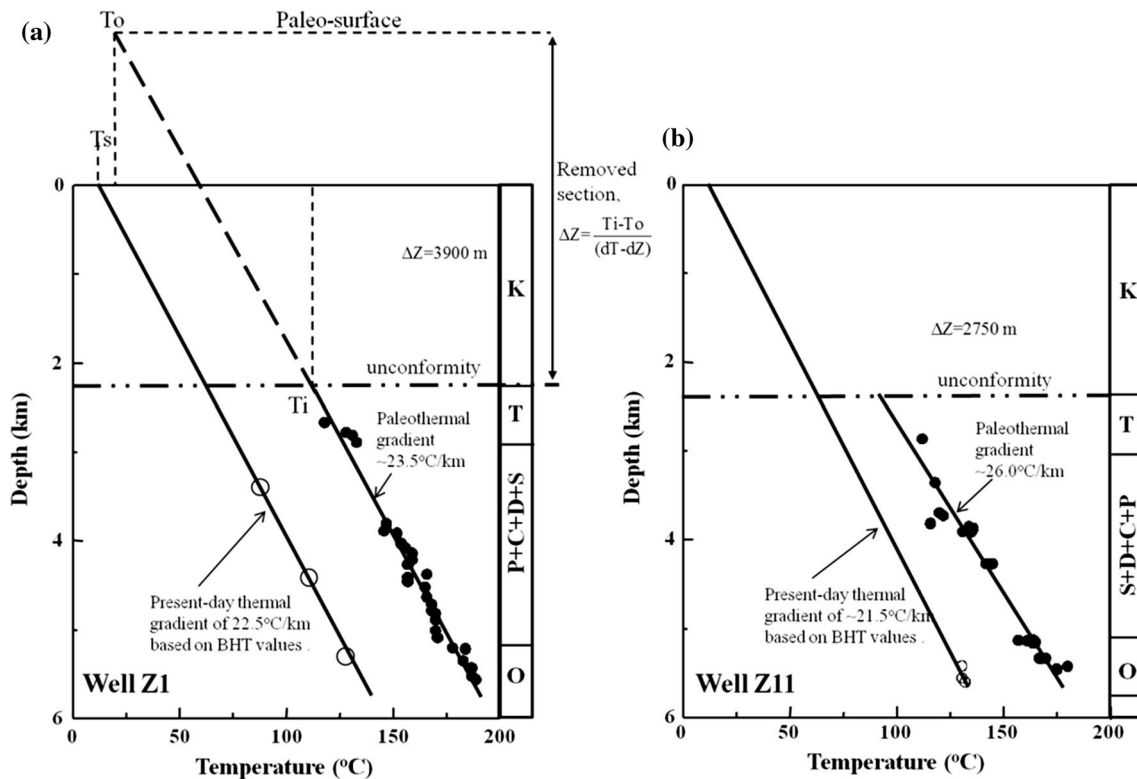


**Fig. 4** Paleo-temperatures derived from  $R_o$  or  $R_{equ}$  in the wells Z1 (a) and Z11 (b) plotted against sample depth. The method of calculating the paleo-geothermal gradient and the amount of erosion from the paleo-temperatures were shown in *left figure* (Bray et al. 1992; Green

et al. 2002). The *empty circles* represent the testing temperatures, and the *dark circles* were paleo-temperatures calculated from the measure  $R_o$  or  $R_{equ}$  data

analysis and hydrocarbon exploration because of its range of annealing temperatures, which is generally considered to be from 60 °C to  $110 \pm 10$  °C, and which approximately corresponds with liquid hydrocarbon generation temperatures over geologic time scales (e.g., Green et al. 1989; Logan and Duddy 1998). Apatite fission track ages, in combination with track length distributions, can provide important constraints for thermal history assessments in sedimentary basins.

Seven samples were collected from sedimentary rocks (sandstone) in well Z2 for studying the Mesozoic cooling history of the Central Tarim (Fig. 1c). Apatite grains were separated from the collected samples using conventional heavy liquid and magnetic separation techniques. The AFT ages and lengths were examined at the China University of Geosciences, Beijing, using the external detector method described by Yuan et al. (2007). The apatite grains were mounted in epoxy resin on glass slides, ground, and polished to an optical finish to expose internal grain surfaces. Mounts were etched in 5.5 Mol  $\text{HNO}_3$  for 20 s at 21 °C to reveal the tracks. Neutron irradiation was carried out in the reactor of China Institute of Atomic Energy at Beijing. Neutron fluence was monitored using the CN5

standard glass. As an external detector, low-U muscovite was etched in 48 % HF for 20 min at 25 °C after irradiation to reveal induced tracks. Track counting and horizontal confined track length measurements were processed on a Zeiss Axiotron microscope under reflected or transmitted light at 1000× magnification. Only those crystals with prismatic sections parallel to the *c*-crystallographic axis were accepted for analysis. Meanwhile, some measured crystal grains with small cracks or dirty polishing surfaces were excluded for each sample. Durango samples were used for determining the zeta calibration. Fission track ages were calculated by the IUGS-recommended zeta calibration approach (Hurford and Green 1982; Hurford 1990) using a zeta value of  $389.4 \pm 19.2$  for the samples. Sample information and the results of the analyses are listed in Table 2.

Single-grain AFT ages and central or pooled ages for all the samples were much younger than the respective stratigraphic ages (Figs. 5, 6a; Table 2). According to the amounts of erosion from  $R_o$  data (3900 and 2750 m) and residual amounts of the overlying strata (Fig. 6), it is probable that all the samples from the well Z2 experienced higher temperature than  $110 \pm 10$  °C. Therefore, we considered that these samples experienced total annealing after

**Table 2** AFT data of the samples from the wells in the Central Tarim

Sample number	No. crystals	Depth (m)	Depositional age	Lithology	$\rho_x$ ( $10^5/\text{cm}^2$ ) ( $N_x$ )	$\rho_y$ ( $10^5/\text{cm}^2$ ) ( $N_y$ )	$\rho_z$ ( $10^5/\text{cm}^2$ ) ( $N_z$ )	$\rho_d$ ( $10^5/\text{cm}^2$ ) ( $N_d$ )	$P(\chi^2)$ (%)	Age (Ma) ( $\pm 1\sigma$ )	Mean track length ( $\mu\text{m}$ ) ( $N$ )	$D_{\text{par}}$ ( $\mu\text{m}$ )
Z2-2	22	2554	Early Triassic (230–250 Ma)	Sandstone	7.512 (1643)	8.820 (1929)	9.761 (5895)	9.761 (5895)	49.36	159 $\pm$ 10	12.5 $\pm$ 1.5 (102)	2.13
Z2-3	23	2963	Early Triassic (230–250 Ma)	Sandstone	5.878 (1433)	7.215 (1759)	9.682 (5895)	9.682 (5895)	86.61	152 $\pm$ 9	12.1 $\pm$ 1.5 (107)	2.07
Z2-7	23	4734	Late Devonian (370–350 Ma)	Sandstone	1.113 (384)	4.446 (1534)	9.604 (5895)	9.604 (5895)	58.1	47 $\pm$ 4	9.6 $\pm$ 1.5 (5)	1.84
Z2-8	22	4805	Late Devonian (370–350 Ma)	Sandstone	1.539 (264)	7.037 (1207)	9.525 (5895)	9.525 (5895)	95.31	41 $\pm$ 3	11.4 $\pm$ 2 (13)	1.95
Z2-9	7	4963	Early Silurian (420–438 Ma)	Sandstone	1.071 (50)	5.097 (238)	9.446 (5895)	9.446 (5895)	20.39	39 $\pm$ 6	10.4 $\pm$ 1.5 (19)	2.01
Z2-10	20	5138	Early Silurian (420–438 Ma)	Sandstone	2.853 (272)	10.351 (987)	9.367 (5895)	9.367 (5895)	21.49	52 $\pm$ 5	10.9 $\pm$ 1.5 (13)	1.76
Z2-11	8	5379	Late Ordovician (438–460 Ma)	Sandstone	4.096 (153)	12.127 (453)	9.288 (5895)	9.288 (5895)	9.53	59 $\pm$ 8	10.0 $\pm$ 1.1 (7)	1.98
TZ10-1 <sup>a</sup>	28	2484	Triassic (205–250 Ma)	Sandstone	5.854 (3047)	2.106 (1096)	1.966 (3144)	1.966 (3144)	3.4	105 $\pm$ 6	12.0 $\pm$ 1.6 (96)	–
TZ10-2 <sup>b</sup>	15	2884	Triassic (205–250 Ma)	Sandstone	12.728 (1368)	15.240 (1638)	–	–	8	91.3 $\pm$ 1.1	11.7 $\pm$ 1.5 (143)	–
TZ10-3 <sup>a</sup>	28	2889	Triassic (205–250 Ma)	Sandstone	7.859 (3087)	2.200 (864)	1.945 (3144)	1.945 (3144)	33.7	133 $\pm$ 7	11.5 $\pm$ 1.5 (98)	–
TZ10-2 <sup>b</sup>	13	3935	Carboniferous (290–350 Ma)	Sandstone	19.223 (1277)	21.316 (1416)	–	–	34	98.5 $\pm$ 1.3	9.8 $\pm$ 1.7 (120)	–
TZ10-3 <sup>b</sup>	8	4162	Carboniferous (290–350 Ma)	Sandstone	3.238 (144)	13.447 (598)	–	–	25	26.5 $\pm$ 1.3	8.8 $\pm$ 2.0 (111)	–
TC1-1 <sup>c</sup>	27	3747	Carboniferous (290–350 Ma)	Sandstone	2.391 (681)	4.827 (1375)	8.983 (3593)	8.983 (3593)	0	96.5 $\pm$ 8.9	9.8 $\pm$ 1.4 (104)	–
TC12-1 <sup>c</sup>	27	4022	Carboniferous (290–350 Ma)	Sandstone	2.716 (578)	4.751 (1011)	8.983 (3593)	8.983 (3593)	0	113.8 $\pm$ 13.4	9.8 $\pm$ 1.4 (87)	–
TZ12-2 <sup>c</sup>	27	4150	Silurian (410–438 Ma)	Sandstone	4.852 (1030)	7.033 (1493)	8.983 (3593)	8.983 (3593)	0	116.7 $\pm$ 16.9	9.7 $\pm$ 1.5 (114)	–
TZ12-3 <sup>c</sup>	26	4254	Silurian (410–438 Ma)	Sandstone	4.017 (540)	9.016 (1212)	8.983 (3593)	8.983 (3593)	0	88.9 $\pm$ 13.3	9.4 $\pm$ 1.5 (71)	–
TZ12-4 <sup>c</sup>	27	4413	Silurian (410–438 Ma)	Sandstone	2.020 (674)	6.055 (2020)	8.983 (3593)	8.983 (3593)	0	66.0 $\pm$ 11.3	9.9 $\pm$ 1.6 (73)	–
TZ8-1 <sup>a</sup>	28	3173	Carboniferous (290–350 Ma)	Sandstone	3.237 (966)	1.280 (382)	1.797 (3144)	1.797 (3144)	47.5	86 $\pm$ 7	9.9 $\pm$ 1.8 (98)	–
TZ8-2 <sup>a</sup>	28	3679	Carboniferous (290–350 Ma)	Sandstone	1.020 (442)	1.389 (602)	1.987 (3144)	1.987 (3144)	52.9	28 $\pm$ 2	9.8 $\pm$ 1.7 (75)	–
TZ6-1 <sup>a</sup>	28	3329	Carboniferous (290–350 Ma)	Sandstone	5.72 (1878)	3.73 (1225)	1.691 (3144)	1.691 (3144)	0	51 $\pm$ 5	10.3 $\pm$ 2.0 (105)	–
TZ6-2 <sup>a</sup>	28	3716	Carboniferous (290–350 Ma)	Sandstone	1052 (528)	1.735 (871)	2.134 (3144)	2.134 (3144)	83.1	25 $\pm$ 2	9.7 $\pm$ 1.7 (80)	–
TZ6-3 <sup>a</sup>	25	3828	Carboniferous (290–350 Ma)	Sandstone	1.819 (573)	2.923 (921)	2.071 (3144)	2.071 (3144)	0	28 $\pm$ 4	10.1 $\pm$ 1.7 (38)	–
TZ18-1 <sup>a</sup>	20	2305	Carboniferous (290–350 Ma)	Sandstone	5.673 (1916)	1.655 (559)	1.649 (3144)	1.649 (3144)	72.2	108 $\pm$ 7	12.2 $\pm$ 2.0 (105)	–
TZ401-1 <sup>a</sup>	22	3312	Carboniferous (290–350 Ma)	Sandstone	5.79 (802)	2.83 (392)	2.050 (3144)	2.050 (3144)	88.3	80 $\pm$ 6	10.7 $\pm$ 1.6 (49)	–



**Table 2** continued

Sample number	No. crystals	Depth (m)	Depositional age	Lithology	$\rho_s$ ( $10^5/\text{cm}^2$ ) ( $N_s$ )	$\rho_1$ ( $10^5/\text{cm}^2$ ) ( $N_1$ )	$\rho_d$ ( $10^5/\text{cm}^2$ ) ( $N_d$ )	$P(\chi^2)$ (%)	Age (Ma) ( $\pm 1\sigma$ )	Mean track length ( $\mu\text{m}$ )	$D_{\text{par}}$ ( $\mu\text{m}$ )
TZ401-2 <sup>a</sup>	27	3697	Carboniferous (290–350 Ma)	Sandstone	1.20 (400)	1.22 (406)	1.934 (3144)	82.8	36 $\pm$ 3	9.6 $\pm$ 2.0 (63)	–
TZ401-3 <sup>a</sup>	28	3712	Carboniferous (290–350 Ma)	Sandstone	1.89 (594)	1.29 (406)	1.902 (3144)	0.3	57 $\pm$ 6	9.4 $\pm$ 2.0 (104)	–
TZ401-4 <sup>a</sup>	28	3735	Carboniferous (290–350 Ma)	Sandstone	3.49 (952)	1.972 (538)	1.881 (3144)	7.4	67 $\pm$ 6	9.3 $\pm$ 1.7 (81)	–

For Age, it means central age when  $P(\chi^2) > 5\%$ , the pooled age is used while  $P(\chi^2) < 5\%$

$D_{\text{par}}$  is the arithmetic mean fission track etch figure diameter parallel to the crystallographic  $c$ -axis

$\rho_s$ , spontaneous track density;  $N_s$ , number of spontaneous tracks;  $\rho_1$ , induced track density in the external detector ( $\rho_d$ );  $N_1$ , number of induced tracks;  $\rho_d$ , induced density in the external detector;  $N_d$ , number of tracks counted in determining  $\rho_d$ ;  $P(\chi^2)$ , Chi square probability

<sup>a</sup> Data were firstly published by Xiang et al. (2013)

<sup>b</sup> Data were firstly published by Qiu et al. (1997)

<sup>c</sup> Data were firstly published by Li et al. (2004)

deposition in the Central Tarim. AFT ages of  $159 \pm 10$  and  $152 \pm 9$  Ma were recorded by the Triassic samples Z2-2 and Z2-3 and revealed the Jurassic cooling event, while other samples had AFT ages of 41–59 Ma, probably related to Paleogene cooling events (Fig. 6a). The mean track lengths of these samples became shorter with elevated temperature and depth (Fig. 6b), indicating that the deeper samples experienced stronger annealing compared with the shallow samples.

We plotted the AFT ages against mean track lengths by combining the AFT ages in this study with previously published AFT data (Fig. 7; Qiu et al. 1997; Li et al. 2004; Xiang et al. 2013). In total, AFT ages range from 25 to 159 Ma and mean track lengths range from 7.8 to 12.9  $\mu\text{m}$  for the samples in the Central Tarim. A typical boomerang trend phenomenon, as reported by Green (1986), is seen in Fig. 7 and indicates that the Central Tarim experienced multiple cooling events in its geologic history.

### Thermal modeling and burial history construction

The timing and magnitude of cooling events in the Central Tarim can be readily revealed by thermal modeling of AFT data. In this paper, the HeFTy software developed by Ketcham (2005) was used to model the thermal history of the Central Tarim with the multi-kinetic annealing model proposed by Ketcham et al. (2007), for which the mean  $D_{\text{par}}$  was a kinetic parameter. Rahn and Seward (2000) suggested that 100 or more measured track lengths are necessary to obtain high-reliability modeling results for one sample, therefore only samples Z2-2 and Z2-3 were used to model the Central Tarim thermal history in this study. The initial modeling time was the time when each sample was deposited in the Central Tarim. The present-day temperature for the model was calculated from the surface temperature (approximately 12 °C) and the bottom hole temperature (BHT) (Fig. 6a). We assumed that the initial surface temperature was 20 °C (Meijun et al. 2010). The program requires some constrained time–temperature intervals. On the basis of the Lower Triassic–Lower Cretaceous and Lower Cretaceous–Paleocene unconformities (Fig. 2b) and measured AFT ages, constraints were chosen around the Early Jurassic and Late Cretaceous. In our modeling, 100,000 thermal paths were developed using a Monte Carlo inverse modeling method, with the best temperature path indicating the thermal history of the sample. Ideally, additional attempted path simulations will give a better thermal interpretation, but 100,000 simulations are sufficient to have a reasonably well-constrained interpretation. Sedimentation, uplift, or erosion would have produced changes in the paleo-temperature of the strata.

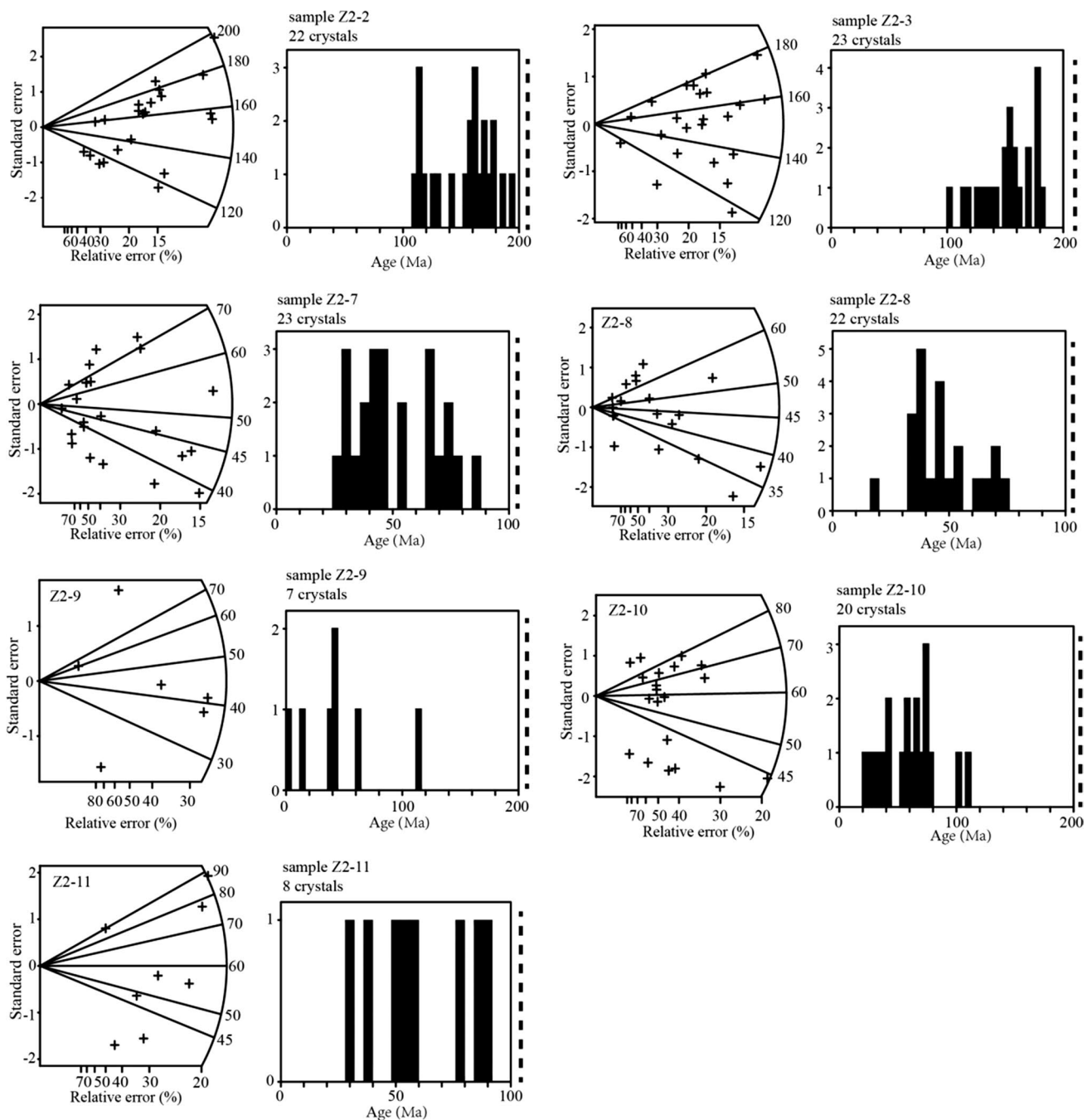


**Fig. 5** Radial plots and age spectra of the samples from the well Z2 in the Central Tarim. The *dash line* in each age spectra represents the depositional age of the sample, indicating that the single-grain AFT ages of all the samples were younger than the corresponding depositional ages

Thermal modeling results for samples Z2-2 and Z2-3 reveal two rapid cooling events, in the Early Jurassic–Early Cretaceous (190–140 Ma) and the Late Cretaceous–Early Paleocene (80–45 Ma) (Fig. 8). The subsidence (heating) following each of these two cooling events corresponded to the residual Lower Cretaceous and Upper Paleozoic–Quaternary strata in well Z2 (Figs. 2b, 6a). The Early Jurassic–Early Cretaceous cooling event

was also revealed by zircon fission track (ZFT) ages in the Bachu Uplift, along the northern margin of the Central Tarim (Fig. 1c; Chang et al. 2014). Meanwhile, Xiao et al. (2011) reported some AFT ages of 134.5–164 Ma from the Kongquehe Slope in the Eastern Tarim Basin. These studies implied that the Early Jurassic–Early Cretaceous cooling event probably influenced the whole Tarim Basin. The Late Cretaceous–Early Paleocene

**Fig. 6** Measured apatite fission track ages (*left*) and length (*right*) profiles with the sample depth for the well Z2 in the Central Tarim

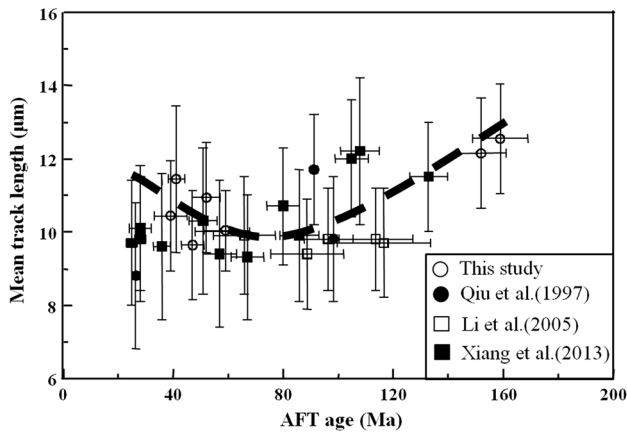
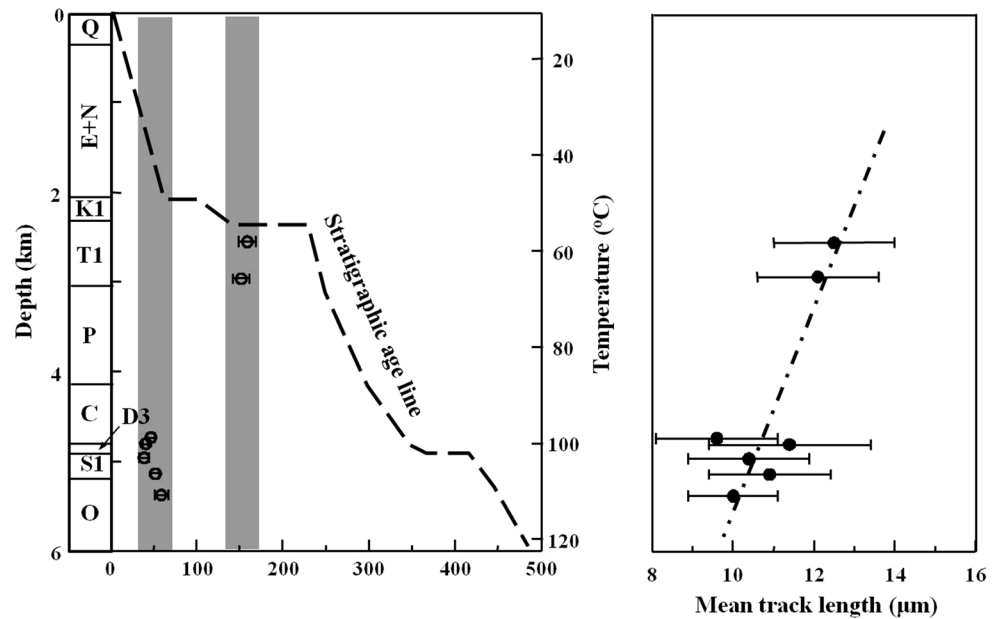


**Fig. 7** AFT ages plotted against mean track lengths for AFT data used in this study and previous studies by Qiu et al. (1997), Li et al. (2004) and Xiang et al. (2013). A typical ‘boomerang’ trend proposed by Green (1986) is shown by the dark dash line

cooling event revealed by thermal modeling of samples Z2-2 and Z2-3 was confirmed by the measured AFT ages of samples Z2-7, Z2-10, Z2-11, TZ12-4, TZ6-1, TZ401-1, TZ401-3, and TZ401-4, and the unconformity between Lower Cretaceous and Paleocene in the Central Tarim (Table 2; Fig. 2b; Li et al. 2004; Xiang et al. 2013). On the basis of decreased temperatures and paleo-geothermal gradients, we calculated the amounts of erosion for these two cooling events as 3000 m in the Early Jurassic–Early Cretaceous and 1600 m in the Late Cretaceous–Early Paleocene (Table 3).

Finally, we reconstructed the burial and thermal history of well Z2 with drilling data and amounts of erosion for these two cooling events, using the Basin Mod 1-D

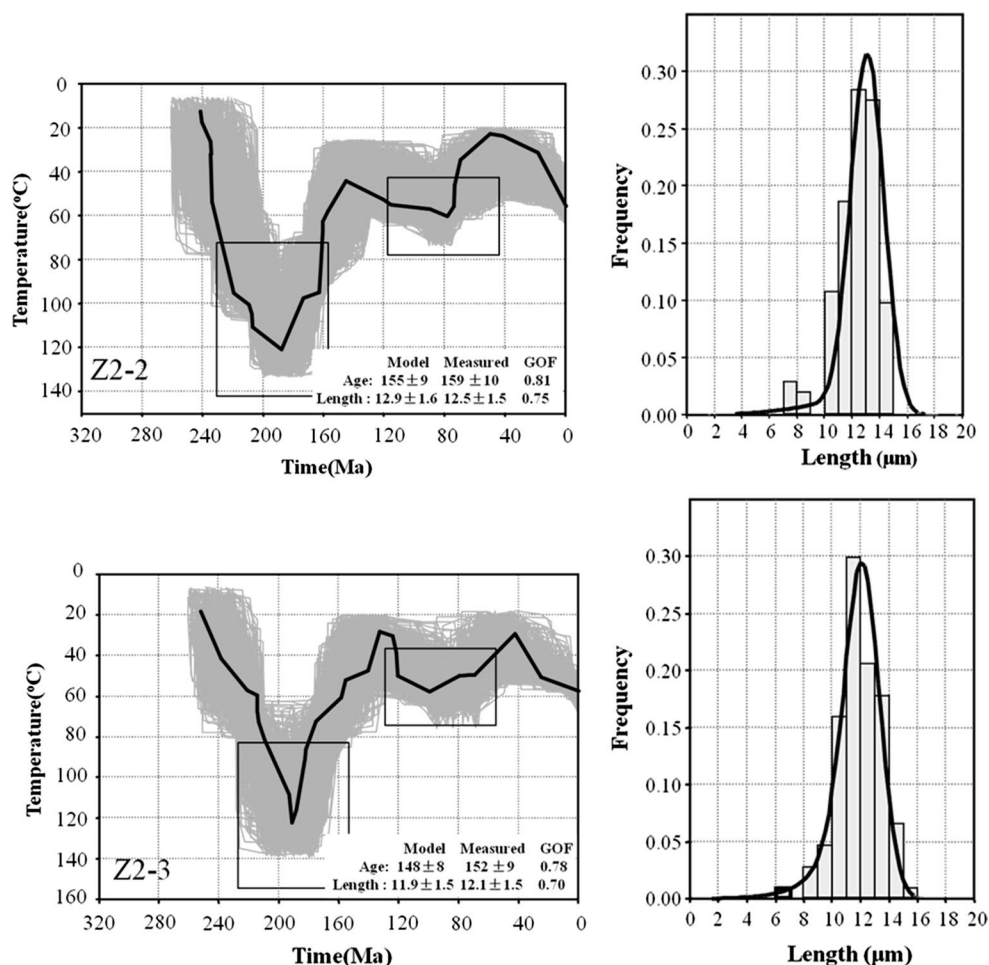
software (Fig. 9). In the modeling, mechanical compaction, coupled with the Falvey and Middleton reciprocal porosity–depth relationship, was used. Figure 9 shows that the modeling results were very consistent with the measured  $R_o$ , which illustrates the reliability of our AFT modeling.

## Discussion

### Tectonic implications for cooling events in the Central Tarim

During the Late Triassic–Early Cretaceous, continuous compressive stress associated with collisions between the Qiangtang–Lhasa Terranes and the southern margin of the Eurasian continent resulted in the formation of several depressions on the margins of the Tarim Basin, such as the Southeast Depression and Southwest Depression. During the Late Triassic–Early Jurassic, the Southwest Depression developed as a foreland basin and accommodated several kilometers of fluvial and lacustrine sediments (Sobel 1999). The Bachu Uplift, close to the northern margin of the Central Tarim, evolved into the forebulge part of this foreland and began to erode seriously from the Early Jurassic to the Early Cretaceous (He et al. 2005; Ding et al. 2008), which was revealed by ZFT ages (Chang et al. 2014). On the basis of AFT data analysis, Zhang et al. (2011a, b) suggested that the Late Jurassic–Early Cretaceous uplift history of the northeastern Tarim Basin was also related to the collision of the Lhasa Terrane with the southern margin of Asia. The Central Tarim evolved into the forebulge part of the Southeast foreland basin because of compressive stress in the Mesozoic and was entirely uplift and then deposited, events

**Fig. 8** Thermal histories of the samples Z2-2 and Z2-3 from the well Z2 by using AFT data. The left figure shows the attempted temperature paths and the thick black line is the best modeled thermal history. The right figure indicates the measured and modeled AFT length distribution. GOF means goodness of fit



that were recorded and revealed by the measured AFT ages and thermal modeling results from samples Z2-2 and Z2-3 in this study and the AFT study of Xiang et al. (2013). Meanwhile, unconformities are further evidence for the Early Jurassic–Early Cretaceous cooling event (Fig. 2b). In addition to collisions on the southern margin of the Eurasia continent, the Early Jurassic–Early Cretaceous cooling event was possibly related to the final accretionary and collisional orogeny of the Chinese Tian Shan northern Tarim Basin during the Mid-Triassic (Xiao et al. 2013), a theory that is supported by the Permian–Triassic titanite fission track and zircon (U–Th)/He data (Glorie et al. 2011).

The measured AFT ages of the samples Z2-7, Z2-10, Z2-11, TZ12-4, TZ6-1, TZ401-1, TZ401-3, and TZ401-4 and the unconformity between Lower Cretaceous and Paleocene in Fig. 2b demonstrated the Central Tarim experienced another cooling event during the Late Cretaceous–Early Paleocene (80–45 Ma), which was also found in the Bachu Uplift, Kuqa Depression, Kuluketage Mountain, and Tian Shan (Wang et al. 2009; Qiu et al. 2011; Zhang et al. 2011a, b; Glorie et al. 2011). The collision of the Dras–Kohistan arc with Eurasia in the Late Cretaceous is

generally considered as the driving force of this cooling event in Central Asia (Zhang et al. 2011a, b; Glorie et al. 2011; Clift et al. 2014). The continuous uplift and erosion during the Early Paleocene in the Central Tarim and other areas were probably related to the collision between the Tibetan–Himalayan microcontinent and the southern margin of Eurasia, which was also called a soft collision between Greater India and Eurasia (van Hinsbergen et al. 2012). This soft collision probably resulted in the crustal shortening of the Tian Shan and the clockwise rotation of the Tarim Block during the Early Cenozoic (Chen et al. 1991). Meanwhile, crustal shortening and convergence of the Tian Shan corresponded to crustal thickening of the Qinghai–Tibet Plateau in the Early Cenozoic (England and Houseman 1986; Deng et al. 2000). In addition, Wang et al. (2008) proposed the distant effects of the soft collision would have reached the East Tian Shan in the Early Cenozoic, based on AFT data. More recent paleomagnetic, biostratigraphic, and sedimentological studies suggested that the final collision of the India plate with Eurasia, which was called a hard collision by van Hinsbergen et al. (2012), occurred around 38–25 Ma (Aitchison et al. 2007;

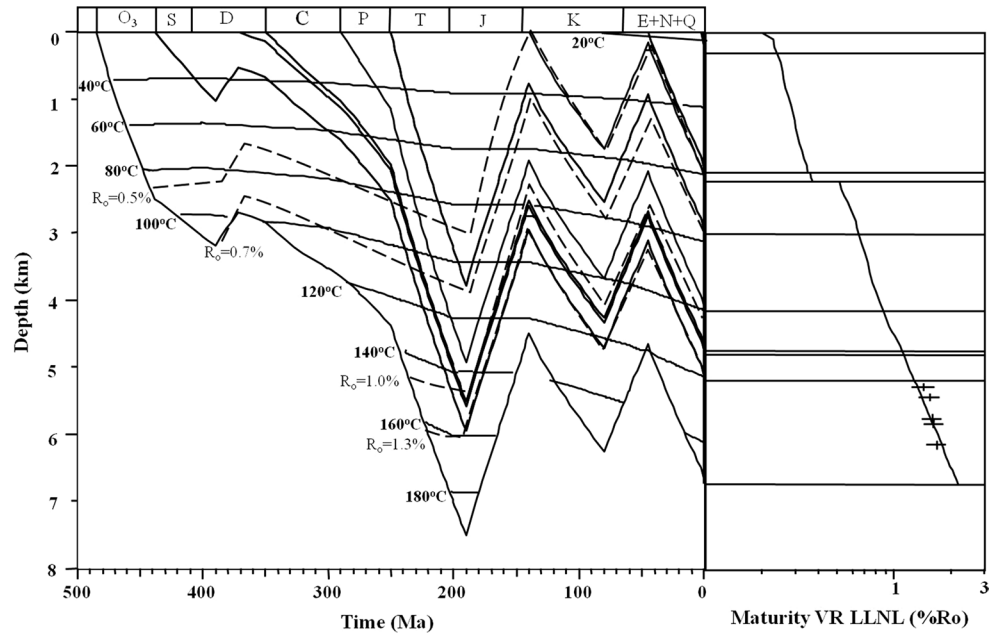
**Table 3** Summary of the cooling events revealed by the thermal modeling

	190–140 Ma			80–45 Ma		
	Decreased temperature	Paleo-geothermal gradient*	Amount of erosion	Decreased temperature	Paleo-geothermal gradient†	Amount of erosion
Z2-2	70	24.8	2800	40	22.0	1800
Z2-3	80	24.8	3200	30	22.0	1400
Mean value			3000			1600

\* Data refer to this study

† Data refer to Li et al. (2004)

**Fig. 9** Reconstructed burial and thermal history of the well Z2 based on the thermal modeling results and drilling data. When reconstructing the thermal history, the paleo-geothermal gradients in the Paleozoic, Mesozoic, and Cenozoic come from the research of Qiu et al. (2012), this study and Li et al. (2004), respectively. The letter “+” means the measured  $R_{\text{equ}}$  data



Jiang et al. 2015). In this study, the measured AFT ages of the samples Z2-8, Z2-9, TZ10-3, TZ8-2, TZ6-2, TZ6-3, and TZ401-2 were consistent with the hard collision time, indicating that the hard collision played an important role on the late uplifting and erosion in the Central Tarim. In addition, the Late Cenozoic cooling event in the northern margin of the Tarim Basin was also probably related to this hard collision (Hendrix et al. 1994; Dumitru et al. 2001; Wang et al. 2009; Zhang et al. 2009; Chang et al. 2012).

### What affected the thermal evolution in the Central Tarim?

In a previous study, Xiang et al. (2013) suggested that heated fluid played an important role in AFT data. However, thermal perturbations caused by heated fluid could not be found for  $R_0$  (or  $R_{\text{equ}}$ ) or AFT data in this study (Bray et al. 1992; Holford et al. 2005). The measured  $R_0$  of wells Z1, Z2, and Z11 showed a linear relationship with

depth (Figs. 4, 9), indicating that there was no heated fluid to increase the  $R_0$ . Sometimes large magmatic events, such as the Emeishan basalt province, can increase  $R_0$  of sedimentary rocks (Zhu et al. 2010). An Early Permian Tarim Large Igneous Province has been systemically studied by field observation, borehole data, zircon U–Pb dating, and geochemical characteristics in the last 5 years (Li et al. 2011, 2012; Yu et al. 2011; Zhang et al. 2013a, b; Xu et al. 2014). However, the 100–300-m thickness of Permian basalts in Z1, Z2, and Z11 wells has no influence on  $R_0$  in older strata (Figs. 4, 9), which indicates that the upwelling and eruption of a mantle plume did not occur in the Central Tarim. According to thermal modeling, Xu et al. (2014) suggested that the Bachu Uplift, with the greatest lithospheric thinning, is a favorable area for an upwelling mantle plume. Since the Mesozoic, the thermal regime in the Central Basin has been mainly dominated by tectonic erosion and deposition, based on AFT and  $R_{\text{equ}}$  analyses in this study.

## Conclusions

We studied the tectono-thermal evolution of the Central Tarim by combining AFT and vitrinite reflectance data. A Mesozoic paleo-geothermal gradient of approximately 24.8 °C/km was obtained from  $R_o$  or  $R_{equ}$  data of Z1 and Z11 wells in the Central Tarim. Measured AFT data and thermal modeling results indicated the presence of Early Jurassic–Early Cretaceous (190–140 Ma) and Late Cretaceous–Paleocene (80–45 Ma) cooling events, in which erosion was 3000 m (consistent with the estimated range of 2700–3900 m from the  $R_o$  or  $R_{equ}$  data) and 1600 m, respectively. These cooling events were related to collisions between the Qiangtang–Lhasa terranes and the Greater India Plate with the southern margin of the Eurasian Plate during the Meso–Cenozoic.

**Acknowledgments** This work was supported by the National Natural Science Foundation of China (No. 41402112, 41125010 and 41072103) and the Science Foundation of China University of Petroleum, Beijing (No. 2462013YJRC034). We are grateful to the Northwest Bureau of Petroleum of SINOPEC which contributed cores and some VR data for this work. We thank Jiang Guang, Qinghua Mei, Yinhui Zuo, Yue Chen and Lu Yun for their help with collecting samples in the field. We thank Zhiyong Zhang and one anonymous reviewer for constructive and helpful reviews that significantly improved the manuscript.

## References

- Aitchison JC, Ali JR, Davis AM (2007) When and where did India and Asia collide? *J Geophys Res* 112:1–19
- Bertrand R, Herous Y (1987) Chitinozoan, Graptolite, and scolecodont reflectance as an alternative to vitrinite and pyrobitumen reflectance in Ordovician and Silurian strata, Anticosti Island, Quebec, Canada. *AAPG Bull* 71:951–957
- Bray RJ, Green PF, Duddy IR (1992) Thermal history reconstruction using apatite fission track analysis and vitrinite reflectance: a case study from the UK East Midlands and Southern North Sea. In: Hardman RFP (ed) *Exploration Britain: Geological insights for the next decade*, vol 67. Geological Society of London, Special Publication, London, pp 3–25
- Buchardt B, Lewan MD (1990) Reflectance of vitrinite-like macerals as a thermal maturity index for Cambrian–Ordovician Alum Shale, southern Scan-dinavia. *AAPG Bull* 74:394–406
- Cai XY (2007) Main factors controlling hydrocarbon accumulation of middle- and large-sized oil and gas fields and their distribution rules in the Tarim Basin. *Oil Gas Geol* 28(6):693–702 (**in Chinese with English abstract**)
- Chang J, Qiu NS, Li JW (2012) Tectono-thermal evolution of the north-western edge of the Tarim Basin in China: constraints from apatite (U–Th)/He thermochronology. *J Asian Earth Sci* 61:187–198
- Chang J, Brown RW, Yuan W, Li W, Que Y, Qiu N (2014) Mesozoic cooling history of the “Bachu Uplift” in the Tarim Basin, China: constraints from zircon fission-track thermochronology. *Radiat Meas* 67:5–14
- Chen Y, Cogne J, Courtillot V, Avouac J, Tapponnier P, Wang G, Bai M, You H, Li M, Wei C, Buffetaut E (1991) Paleomagnetic study of Mesozoic continental sediments along the northern Tien Shan (China) and heterogeneous strain in central Asia. *J Geophys Res* 96:4065–4082
- Clift PD, Carter A, Jonell TN (2014) U–Pb dating of detrital zircon grains in the Paleocene Stumpata Formation, Tethyan Himalaya, Zaskar, India. *J Asian Earth Sci* 82:80–89
- Deng QD, Feng XY, Zhang PZ, Xu XW, Yang XP, Peng SZ, Li J (2000) *The neotectonics of Tien Shan*. Seismological Press, Beijing (**in Chinese**)
- Ding WL, Lin CS, Qi LX, Huang TZ, Yu TX (2008) Structural framework and evolution of Bachu Uplift in Tarim Basin. *Earth Sci Front* 15:242–252 (**in Chinese with English abstract**)
- Dumitru TA, Zhou D, Chang EZ, Graham SA, Hendrix MS, Sobel ER, Carroll AR (2001) Uplifting, exhumation, and deformation in the Chinese Tianshan. In: Hendrix MS, Davis GA (eds) *Paleozoic and Mesozoic tectonic evolution of central Asia: From continental assembly to intracontinental deformation*, vol 194. Geological Society of America Memoir, Colorado, pp 71–99
- England P, Houseman G (1986) Finite strain calculations of continental deformation 2: comparison with the India-Asia collision zone. *J Geophys Res* 91:3664–3676
- Ge R, Zhu W, Wilde SA, He J, Cui X, Wang X, Zheng B (2014) Neoproterozoic to Paleozoic long-lived accretionary orogeny in the northern Tarim Craton. *Tectonics* 33:302–329
- Gleadow AJW, Duddy IR, Lovering JF (1983) Fission track analysis: a new tool for the evaluation of thermal histories and hydrocarbon potential. *APEA J* 23:93–102
- Glorie S, De Grave J, Buslov MM, Zhimulev FI, Stockli DF, Batalev VY, Izmer A, Van den Haute P, Vanhaecke F, Elburg MA (2011) Tectonic history of the Kyrgyz South Tian Shan (Atbashi-Inylchek) suture zone: The role of inherited structures during deformation-propagation. *Tectonics* 30:1–23
- Green PF (1986) On the thermo-tectonic evolution of Northern England: evidence from fission track analysis. *Geol Mag* 123:493–506
- Green PF, Duddy IR, Laslett GM, Hegerly KA, Gleadow AJW, Lovering JF (1989) Thermal annealing of fission tracks in apatite: 4. Quantitative modelling techniques and extension to geological timescales. *Chem Geol* 79:155–182
- Green PF, Duddy IR, Hegarty KA (2002) Quantifying exhumation from apatite fission-track analysis and vitrinite reflectance data: precision, accuracy and latest results from the Atlantic margin of NW Europe. In: Dore AG, Cartwright JA, Stokers MS, Turner JP, White N (eds) *Exhumation of the North Atlantic margin: timing, mechanisms and implications for petroleum exploration*, vol 196. Geological Society of London, Special Publication, London, pp 331–354
- He DF, Jia CZ, Li DS, Zhang CJ, Meng QR, Shi X (2005) Formation and evolution of polycyclic superimposed Tarim Basin. *Oil Gas Geol* 26:64–77 (**in Chinese with English abstract**)
- He ZL, Chen QL, Qian YX, Li HL (2006) Hydrocarbon exploration targets in central uplift area of Tarim Basin. *Oil Gas Geol* 27:769–778 (**in Chinese with English abstract**)
- Hendrix MS, Dumitru TA, Graham SA (1994) Late Oligocene-early Miocene unroofing in the Chinese Tian Shan: an early effect of the India-Asia collision. *Geology* 22:487–490
- Holford SP, Green PF, Turner JP (2005) Palaeothermal and compaction studies in the Mochras borehole (NW Wales) reveal early Cretaceous and Neogene exhumation and argue against regional Palaeogene uplift in the southern Irish Sea. *J Geol Soc Lond* 162:829–840
- Hurfurd AJ (1990) Standardization of fission-track dating calibration: recommendation by the fission track working group of the I. U. G. S. subcommission on geochronology. *Chem Geol* 80:171–178
- Hurfurd AJ, Green PF (1982) A users’ guide to fission-track dating calibration. *Earth Planet Sci Lett* 59:343–354
- Jacob H (1989) Classification, structure, genesis and practical importance of natural solid bitumen. *Int J Coal Geol* 11:65–79
- Jia CZ (1997) *Structural feature and petroleum in Tarim Basin*. Petroleum Industry Press, Beijing, China (**in Chinese**)

- Jia CZ, Wei GQ, Yao HJ (1995) Tectonic evolution and regional structural geology: Book series on petroleum exploration in the Tarim Basin. Petroleum Industry Press, Beijing **(in Chinese)**
- Jiang T, Aitchison JC, Wan XQ (2015) The youngest marine deposits preserved in southern Tibet and disappearance of the Tethyan Ocean. *Gondwana Res*. doi:10.1016/j.gr.2015.01.015
- Ketcham RA (2005) Forward and inverse modeling of low-temperature thermochronometry data. *Rev Miner Geochem* 58:275–314
- Ketcham RA, Carter A, Donelick RA, Barbarand J, Hurford AJ (2007) Improved modeling of fission-track annealing in apatite. *Am Miner* 92:799–810
- Li H, Qiu N, Jin Z, Yang H, Li Y (2004) Study on thermal history of Tazhong area, Tarim Basin. *J Xi'an Shiyou Univ (Nat Sci Ed)* 19:36–39 **(in Chinese with English abstract)**
- Li H, Qiu N, Jin Z (2005) Thermal history of central area of the Tarim Basin by apatite fission track analysis. *Chin J Geol* 40:129–132 **(in Chinese with English abstract)**
- Li YJ, Wu GY, Meng QL, Yang HJ, Han JF, Li XS, Dong LS (2008) Fault systems in central area of the Tarim Basin: geometry, kinematics and dynamic settings. *Chin J Geol* 43:82–118 **(in Chinese with English abstract)**
- Li BL, Guan SW, Li CX, Wu GH, Yang HJ, Han JF, Luo CS, Miao JJ (2009) Paleo-tectonic evolution and deformation features of the Lower Uplift in the Central Tarim Basin. *Geol Rev* 55:521–529 **(in Chinese with English abstract)**
- Li SM, Pang XQ, Jin ZJ, Yang HJ, Xiao ZY, Gu QY, Zhang BS (2010) Petroleum source in the Tazhong Uplift, Tarim Basin: new insights from geochemical and fluid inclusion data. *Org Geochem* 41:531–553
- Li ZL, Chen HL, Song BA, Li YQ, Yang SF, Yu X (2011) Temporal evolution of the Permian large igneous province in Tarim Basin in northwestern China. *J Asian Earth Sci* 42:917–927
- Li ZL, Li YQ, Chen HL, Santosh M, Yang SF, Xu YG, Langmuir CH, Chen ZX, Yu X, Zou SY (2012) Hf isotopic characteristics of the Tarim Permian large igneous province rocks of NW China: implication for the magmatic source and evolution. *J Asian Earth Sci* 49:191–202
- Li C, Wang X, Li B, He D (2013) Paleozoic fault systems of the Tazhong Uplift, Tarim Basin, China. *Mar Pet Geol* 39:48–58
- Lin C, Yang H, Liu J, Rui Z, Cai Z, Zhu Y (2012) Distribution and erosion of the Paleozoic tectonic unconformities in the Tarim Basin, Northwest China: significance for the evolution of paleo-uplifts and tectonic geography during deformation. *J Asian Earth Sci* 46:1–19
- Logan P, Duddy I (1998) An investigation of the thermal history of the Ahnet and Reggane Basins, Central Algeria, and the consequences for hydrocarbon generation and accumulation. In: Macgregor DS, Moody RTJ, Clark-lowes DD (eds) *Petroleum Geology of North Africa*, vol 132. Geological Society of London, Special Publication, London, pp 131–155
- Lü XX, Hu X (1997) Hydrocarbon accumulation and distribution in Tazhong Low Uplift of Tarim Basin. *Oil Gas Geol* 19:288–293 **(in Chinese with English abstract)**
- Meijun L, Tieguan W, Jianfa C, Faqi H, Lu Y, Sadik A, Weibiao Z (2010) Paleo-heat flow evolution of the Tabei Uplift in Tarim Basin, northwest China. *J Asian Earth Sci* 37:52–66
- Pan CC, Zhou ZY, Fan SF, Xie QL (1996) Thermal history of Tarim Basin. *Bull Miner Pet Geochem* 15:150–177 **(in Chinese with English abstract)**
- Qiu N, Jin Z, Wang F (1997) The effect of the complex geothermal field based on the multi-structure evolution to hydrocarbon generation- a case of Tazhong Area in Tarim Basin. *Acta Sedimentol Sin* 15:142–144 **(in Chinese with English abstract)**
- Qiu NS, Jiang G, Mei QH, Chang J, Wang SJ, Wang JY (2011) The Paleozoic tectonothermal evolution of the Bachu Uplift of the Tarim Basin, NW China: constraints from (U–Th)/He ages, apatite fission track and vitrinite reflectance data. *J Asian Earth Sci* 41(6):551–563
- Qiu N, Chang J, Zuo Y, Wang J, Li H (2012) Thermal evolution and maturation of Lower Paleozoic source rocks in the Tarim Basin, northwest China. *AAPG Bull* 96:789–821
- Rahn M, Seward D (2000) How many track lengths do we need? *Ontrack* 20:12–15
- Sobel E (1999) Basin analysis of the Jurassic–Lower Cretaceous southwest Tarim Basin, Northwest China. *GSA Bull* 111:709–724
- Sobel E, Chen J, Heermance R (2006) Late Oligocene–Early Miocene initiation of shortening in the Southwestern Chinese Tian Shan: implications for Neogene shortening rate variations. *Earth Planet Sci Lett* 247(1–2):70–81
- Stach E, Mackowsky MT, Teichmüller M, Taylor GH, Chandra D, Teichmüller R (1982) *Stach's Textbook of coal petrology*, 3rd edn. Gebrüder Borntraeger, Berlin
- Sweeney JJ, Burnham AK (1990) Evaluation of a simple model of vitrinite reflectance based on chemical kinetics. *AAPG Bull* 74:1559–1570
- Tissot BP, Welte DH (1978) *Petroleum formation and occurrence: A new approach to oil and gas exploration*. Springer, Berlin
- van Hinsbergen DJJ, Lippert PC, Dupont-Nivet G, McQuarrie N, Doubrovine PV, Spakman W, Torsvik TH (2012) Greater India Basin hypothesis and a two-stage Cenozoic collision between India and Asia. *Proc Natl Acad Sci USA* 109(20):7659–7664
- Wang FY, He P, Cheng DS, Hao SS, Liu DH (1996) Vitrinite-like reflectance research on Lower-Paleozoic high- and post-mature source rocks. *Nat Gas Ind* 16(4):14–18 **(in Chinese with English abstract)**
- Wang ZY, Lu KZ, Qi JF, Jin ZJ, Lu XX (1998) Relation between tectonic evolution and oil–gas reservoir in Tazhong Uplift of Tarim Basin. *J Univ Pet China* 22:14–17 **(in Chinese with English abstract)**
- Wang ZX, Li T, Zhang J, Liu YQ, Ma ZJ (2008) The uplifting process of the Bogda Mountain during the Cenozoic and its tectonic implication. *Sci China Ser D Earth Sci* 51:579–593
- Wang QC, Li SJ, Du ZL (2009) Differential uplift of the Chinese Tianshan since the Cretaceous: constraints from sedimentary petrography and apatite fission-track dating. *Int J Earth Sci* 98:1341–1363
- Wang TG, Dai SF, Li MJ, Zhang WB, Qiu NS, Wang GL (2010) Stratigraphic thermohistory and its implications for regional geoevolution in the Tarim Basin, NW China. *Sci China Earth Sci* 53:1495–1505
- Wu GH, Li HW, Xu YL, Su W, Chen ZY, Zhang BS (2012) The tectonothermal events, architecture and evolution of Tarim craton basement palaeo-uplifts. *Acta Petrol Sin* 28:2435–2452
- Xiang C, Pang X, Danisik M (2013) Post-Triassic thermal history of the Tazhong Uplift in the Tarim Basin, Northwest China: evidence from apatite fission-track thermochronology. *Geosci Front* 4:743–754
- Xiao H, Ren ZL, Wang QC, Zhao JZ (2011) Detrital zircon and apatite fission track study of key tectonic events of Kongquehe slope and Kuruketage uplift, north-eastern Tarim Basin, China. *Chin J Geophys* 54(3):817–827
- Xiao WJ, Windley BF, Allen MB, Han CM (2013) Paleozoic multiple accretionary and collisional tectonics of the Chinese Tianshan orogenic collage. *Gondwana Res* 23:1316–1341
- Xie QL, Zhou ZY (2002) Kerogen pyrolysis kinetics simulating experiment used to study Low Paleozoic paleotemperature in Tarim Basin. *Earth Sci J China Univ Geosci* 27:767–769 **(in Chinese with English abstract)**
- Xu YG, Wei X, Luo ZY, Liu HQ, Cao J (2014) The Early Permian Tarim Large Igneous Province: main characteristics and a plume incubation model. *Lithos* 204:20–35

- Yang S, Chen H, Ji D, Li Z, Dong C, Jia C, Wei G (2005) Geological Process of Early to Middle Permian Magmatism in Tarim Basin and its geodynamic significance. *Geol J China Univ* 11(4):504–511 (in Chinese with English abstract)
- Yu X, Yang SF, Chen HL, Chen ZQ, Li ZL, Batt GE, Li YQ (2011) Permian flood basalts from the Tarim Basin, Northwest China: SHRIMP zircon U–Pb dating and geochemical characteristics. *Gondwana Res* 20(2–3):485–497
- Yuan WM, Bao ZK, Dong JQ, Guo ZJ, Deng J (2007) Zircon and apatite fission track analyses on mineralization ages and tectonic activities of Tuwu-Yandong porphyry copper deposit in northern Xinjiang, China. *Sci China Ser D Earth Sci* 50:1787–1795
- Zhang GY (2000) The formation and evolution of the Tarim cratonic basin in Paleozoic and its Hydrocarbon. Geological Publishing House, Beijing (in Chinese)
- Zhang ZY, Zhu WB, Shu LS, Wan JL, Yang W, Su JB, Zheng BH (2009) Apatite fission track thermochronology of the Precambrian Aksu blueschist, NW China: implications for thermo-tectonic evolution of the north Tarim basement. *Gondwana Res* 16(2):182–188
- Zhang Y, Zwingmann H, Liu K, Todd A, Luo X (2011a) Hydrocarbon charge history of the Silurian bituminous sandstone reservoirs in the Tazhong Uplift, Tarim Basin, China. *AAPG Bull* 95:395–412
- Zhang ZY, Zhu WB, Shu LS, Wan JL, Yang W, Zheng BH, Su JB (2011b) Multi-stage exhumation of the NE Tarim Precambrian bedrock, NW China: constraints from apatite fission track thermochronology in the Kuluketage area. *Terra Nova* 23:324–332
- Zhang CL, Zou HB, Li HK, Wang HY (2013a) Tectonic framework and evolution of the Tarim Block in NW China. *Gondwana Res* 23:1306–1315
- Zhang DY, Zhang ZC, Santosh M, Cheng ZG, He H, Kang JL (2013b) Perovskite and baddeleyite from kimberlitic intrusions in the Tarim large igneous province signal the onset of an end-Carboniferous mantle plume. *Earth Planet Sci Lett* 361:238–248
- Zhu C, Xu M, Yuan Y, Zhao Y, Shan J, He Z, Tian Y, Hu S (2010) Palaeogeothermal response and record of the effusing of Emeishan basalts in the Sichuan basin. *Chin Sci Bull* 55:949–956